

Recruitment of Tendon Crimp With Applied Tensile Strain

Kristi A. Hansen

Jeffrey A. Weiss

Department of Bioengineering,
The University of Utah,
50 S Central Campus Dr #2480,
Salt Lake City, UT 84112

Jennifer K. Barton

Biomedical Engineering Program,
The University of Arizona,
1230 E. Speedway Blvd.,
Tucson, AZ 85721

The tensile stress-strain behavior of ligaments and tendons begins with a toe region that is believed to result from the straightening of crimped collagen fibrils. The in situ mechanical function is mostly confined to this toe region and changes in crimp morphology are believed to be associated with pathological conditions. A relatively new imaging technique, optical coherence tomography (OCT), provides a comparatively inexpensive method for nondestructive investigation of tissue ultrastructure with resolution on the order of 15 μm and the potential for use in a clinical setting. The objectives of this work were to assess the utility of OCT for visualizing crimp period, and to use OCT to determine how crimp period changed as a function of applied tensile strain in rat tail tendon fascicles. Fascicles from rat tail tendons were subjected to 0.5 percent strain increments up to 5 percent and imaged at each increment using OCT. A comparison between OCT images and optical microscopy images taken between crossed polarizing lenses showed a visual correspondence between features indicative of crimp pattern. Crimp pattern always disappeared completely before 3 percent axial strain was reached. Average crimp period increased as strain increased, but both elongation and shortening occurred within single crimp periods during the application of increasing strain to the fascicle.

[DOI: 10.1115/1.1427698]

Keywords: Collagen, Fascicle, Fibril, Optical Coherence Tomography, Material Properties

Introduction

The relationship between tissue microstructure and continuum level function has long been a topic of interest in biomechanics and tissue engineering. The material properties of biological tissues depend on the component materials and structural organization from the microscopic to macroscopic level. Due to difficulties in accurately visualizing tissue microstructure, studies of structure-function relations in biological soft tissues are often difficult or impossible. Although histological methods can provide some microstructural information, these techniques require destruction of the tissue and often alter the relationship between tissue components.

The material behavior of tendons and ligaments is important in the study of injury, reconstruction, and surgical techniques. Knowledge of the tissue structure and organization can enhance this understanding. Although there are subtle differences in the organization of different tendons and ligaments, the rat tail tendon has been studied extensively as a model tissue. Tail tendons are composed of several fascicles, which in turn consist of fibrils (Fig. 1) [1–4]. A crimp or banding pattern can be readily observed in histological preparations of rat tail fascicles via polarized light microscopy. Rigby et al. [5] and Diamant et al. [6] observed that crimp pattern disappears above 4 percent strain. The point at which the crimp disappears is referred to as the point of crimp extinction. The stress-strain behavior of fascicle is nonlinear prior to the disappearance of the crimp, forming a “toe region” in the stress-strain curve. The physiological function of tendon is mostly confined to this toe region [7].

Several models of structural organization have been proposed for the rat tail tendon. Diamant et al. [6] used optical microscopy (OM) to demonstrate the planarity of a zigzag crimp waveform inherent in fascicle fibrils. Kastelic et al. [1] proposed that fascicles have a cylindrical array of planar zigzag crimped fibrils based on interpretation of OM and scanning electron microscopy

(SEM) studies. Niven et al. [2] presented a structural model based on a triangular cross-sectional shape with planes of crimped fascicles packed parallel to the longest edge of the triangle. Rowe [3,4] used OM and SEM to develop a rat tail tendon fascicle model that suggested that the waveforms of collagen fibrils assemble side-by-side with a degree of freedom in any direction in the register of the wave. Regardless of the exact fibril organization, all previous investigations are in agreement that the fascicles form a wavy configuration, or crimp pattern, with variable periodicity. Studies have also demonstrated that the band width seen in OM pictures is directly related to the crimp period that is measured using histological techniques [4,5,8]. Gathercole and Keller summarized their 18 years of work by noting that “alterations in crimp structure are symptoms, or even causes, of pathological conditions.”

In addition to OM, a number of nondestructive techniques have been applied to the quantification of soft tissue microstructure. Sacks et al. [9] used a small angle light scattering device to measure fiber orientation in planar fibrous connective tissue of less than 500 μm thickness with an angular resolution of approximately 1 deg and a spatial resolution of $\pm 254 \mu\text{m}$. Magnetic resonance diffusion tensor microscopy was used to measure fiber orientation in canine myocardium [10] and the lamellar structure of the intervertebral disk [11]. Caspers et al. [12] used Raman spectroscopy to investigate the composition of the layers of skin. Optical coherence tomography (OCT) provides a relatively inexpensive, nondestructive alternative for the analysis of soft tissue microstructure, with resolution that is superior to the aforementioned techniques in three dimensions (on the order of 15 μm) [13]. OCT is an optical analogue to ultrasound, utilizing reflected near-infrared light instead of sound. The intensity of reflected low coherence light is measured, using a Michelson interferometer to determine its spatial origin. OCT has been used to image biological tissues in vitro and in vivo, including skin [14,15], aorta [16], and tendon [17].

Nondestructive and minimally invasive measurement of the ultrastructure of collagenous soft tissues would provide a unique method for the evaluation of normal and healing tissues and the efficacy of treatment regimens. The technology has the potential

Contributed by the Bioengineering Division for publication in the JOURNAL OF BIOMECHANICAL ENGINEERING. Manuscript received by the Bioengineering Division August 17, 2000; revised manuscript received August 16, 2001. Associate Editor: L. J. Soslowsky.

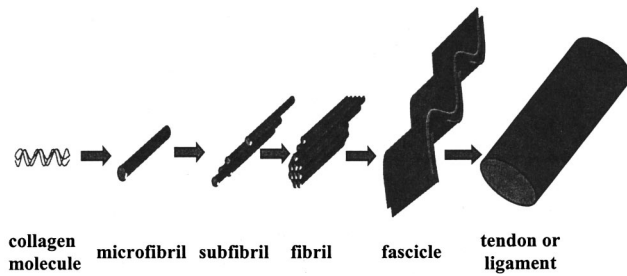


Fig. 1 Schematic illustrating the ultrastructure of rat tail tendon and the level at which crimp is observed within the structural hierarchy. Tendons and ligaments are composed mainly of type I collagen. Collagen molecules form into microfibrils that aggregate to form subfibrils. A number of subfibrils form fibrils, which associate into fibers or fascicles [1]. Fascicles finally assemble to form tendons and ligaments. Crimp is observed at the level of the fascicle.

to be packaged into an arthroscopic probe for clinical use, and could provide quantitative measurements of changes in the ultrastructure of soft tissues that could not otherwise be detected. The technique could also be used to determine microstructural parameters for constitutive models of the tissue material behavior [18,19]. The objectives of this work were to assess the ability of OCT to visualize crimp period, and to use OCT to determine how crimp period changed as a function of applied tensile strain in rat tail tendon fascicles. Our hypotheses were that 1) the crimp bands observed in OCT images of tendon fascicles would correspond to the crimp period measured with OM, 2) the width of crimp bands would increase and the bands would eventually disappear as increasing axial strain was applied, and 3) the average period of sequential, axially aligned crimp bands would increase with increasing strain.

Materials and Methods

Experimental Design and Tissue Preparation. Eight fascicles from five rat tails were imaged with OCT at successive levels of uniaxial tensile strain. Rat tails were obtained immediately following sacrifice, wrapped in 0.9 percent buffered saline wetted gauze, and frozen at -70°C until dissection. Thawed tails were skinned and cut approximately 65 mm from the proximal end. Sections of single fascicles were gently teased from the surrounding epitenon [3] and clamped into a custom-built mechanical testing device (Fig. 2). To preserve the mechanical and optical

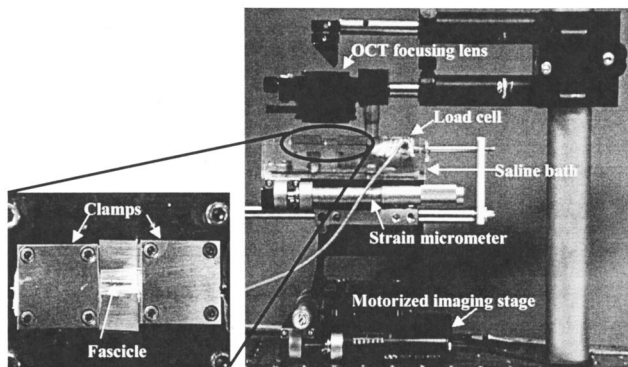


Fig. 2 Mechanical testing device used to apply tensile strain to fascicles while imaging with OCT. The strain micrometer applied incremental changes in axial strain, while the motorized imaging stage was used to acquire the OCT images. Inset shows a close-up of the clamps with a fascicle secured for testing.

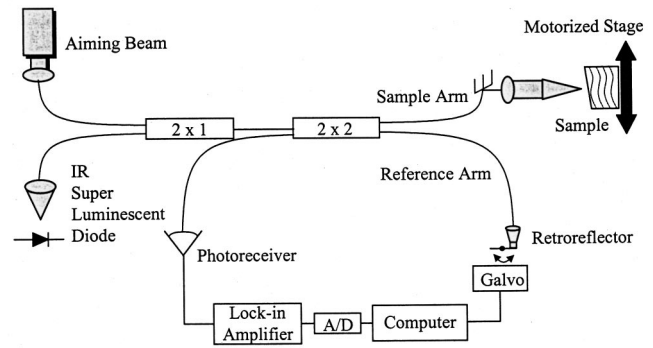


Fig. 3 OCT system schematic. Using Michelson interferometry, backscattered light from the sample and translating retroreflector interferes when the pathlength is within the coherence length of the source.

properties of the tissue, fixatives were not used and fascicles were kept continuously moist with 0.9 percent buffered saline during harvest, preparation, and imaging. A single-monofilament suture (Polyglyconate, 3-0, Davis & Geck Monofil Inc., Manati, PR) was attached with cyanoacrylate to each fascicle, transverse to the collagen fiber direction of the tissue in the central third of the fascicle length (Fig. 2, inset). The suture served as a fiduciary for registration between successive OCT images. Fascicle ends were wrapped in saline-soaked gauze to increase the gripping area and avoid tissue damage. Each fascicle end was secured in a clamp, allowing a small amount of slack to avoid prematurely stretching the tissue. The mechanical test device was then attached to the motorized stage for OCT imaging.

OCT System. The OCT system used a short coherence length source, in this case a superluminescent diode, with a center wavelength of 1290 nm and a bandwidth of 49 nm (Fig. 3). The infrared beam was combined with a red aiming beam and coupled into the source arm of a fiber Michelson interferometer. The interferometer split the light into reference and sample arms. In the sample arm, light was focused onto the tissue. In the reference arm, pathlength modulation was provided by a galvanometer-mounted retroreflector. Light reflected from the reference and sample arms interfered only when the respective pathlengths were within a source coherence length (approximately $16\ \mu\text{m}$). Thus by scanning the retroreflector, a determination of reflectivity versus sample depth (an a-scan) was made. This signal was detected by a photodiode, with an interference fringe frequency dependent upon the speed of the moving retroreflector. A lock-in amplifier demodulated the signal at this frequency and allowed signals weaker than 10^{-5} of the incident light to be detected. A two-dimensional image was created from multiple a-scans acquired while a motorized stage translated the tendon in the lateral direction. The system axial and lateral (in-plane) resolutions, given by the coherence length of the source and the sample beam focus in tissue, were 16 and $14\ \mu\text{m}$, respectively. Each image voxel was $2.8 \times 10.0 \times 10.0$ microns, so the image data were oversampled in comparison to the resolution of the device. Images consisting of 200 a-scans were obtained in approximately 14 s.

Mechanical Test Device and Protocol. The mechanical test device was designed to apply measured increments of uniaxial strain to the fascicles. One clamp was attached to a translation stage and the other was fixed to a stationary plate. A micrometer (accuracy $\pm 5\ \mu\text{m}$) adjusted the position of the translation stage to apply strain to the clamped tissue. An 11.0-N capacity load cell (Transducer Techniques, Temecula, CA, accuracy $\pm 0.055\ \text{N}$) was used to continuously monitor applied load during the application of each strain increment.

The zero-load length of the fascicle was established by con-

secutively applying and removing a small tare load (0.01 N) via adjustment of the micrometer. The clamp-to-clamp distance was then measured with calipers (accuracy $\pm 50 \mu\text{m}$) to determine the zero-load length (l_0). Three OCT images were taken oriented perpendicular to the long axis of the fascicle and spaced 3 mm apart. These images were processed using image analysis software (Scion Corporation, Frederick, MD) to fit an ellipse to the boundary of the fascicle. The areas of the ellipses from the three images were averaged to determine initial cross-sectional area (A_0). The accuracy of this area measurement technique depends on the correspondence between the boundary of the fascicle in the OCT image and the resolution of the OCT image, and the ability of an ellipse to describe the boundary of the fascicle. A conservative estimate of this accuracy is ± 5.0 percent. This is based in part on the error of ± 1 pixel in the determination of the laterally aligned (with respect to the OCT system) ellipse axis and ± 3 pixels for the axially aligned axis of the ellipse, with the ellipse axes typically composed of 36 and 99 pixels, respectively. After acquisition of images for cross-sectional area measurement, the mechanical test device was rotated 90 deg for OCT imaging of the tissue parallel to the fascicle long axis in the zero-load configuration.

The fascicle was consecutively stretched in increments of approximately 0.5 percent clamp-to-clamp strain. The exact incremental change in length (Δl) was recorded in order to calculate clamp-to-clamp engineering strain as $\varepsilon = \Delta l / l_0$. An OCT image was acquired for each strain increment once the load relaxation rate dropped below a value of 0.001 N/s. All longitudinal images included the suture fiduciary. Engineering stress (σ) was calculated at each strain increment using the initial cross-sectional area (A_0) and the measured load (F) at the beginning of each image acquisition as $\sigma = F / A_0$. To determine any differences between clamp-to-clamp strain and tissue level strain, a pilot study was performed using a series of surgical microscope images from single fascicles. The fascicles were placed in the mechanical test device and subjected to the same incremental strain conditions described above. Clamp-to-clamp values of l_0 and Δl were measured as previously stated. In these images the fascicles did not have suture markers but the center third was identified by two thin marks of black stain. Marker-to-marker L_0 and ΔL were measured from the images. The difference between the two strain measures was smaller than the lateral resolution of the OCT system.

Band Pair Relationship to Crimp Period. To determine the relationship between banding and crimp period observed in OM studies [5,6,8] and banding observed in OCT images, three fascicles were obtained from a single rat tail and imaged using OCT and subsequently using an optical microscope (Nikon, SMZ-2T) between crossed polarizers. The ends of each fascicle were adhered to a microscope slide at each end with cyanoacrylate, such that the fascicle was visibly taut. Two monofilament sutures were attached with cyanoacrylate, 4 mm apart and perpendicular to the long axis of the fascicle in the center of the length between adhesion spots. These sutures served as fiducials for registration between corresponding OCT and OM images. The fascicles were kept in a 0.9 percent buffered saline bath at all times.

Longitudinal OCT images were taken along the center of the fascicle with the slide in two separate orientations. One image was taken with the slide perpendicular to the imaging beam axis and the second with the slide parallel to the beam axis. Two OM images were also obtained. In the first image, extinction bands encompassed an entire crimp arm or half of a crimp period [8], such that each OM image band pair width was equivalent to one full crimp period. The second image was taken with the polarizers crossed. These images were used to relate OCT image banding to OM image banding, which has a known relationship to crimp period. OM images and corresponding OCT images were compared visually, side-by-side. Perpendicularly acquired OCT images were compared to each other by their average period.

Data Reduction and Statistical Analysis. The OCT images

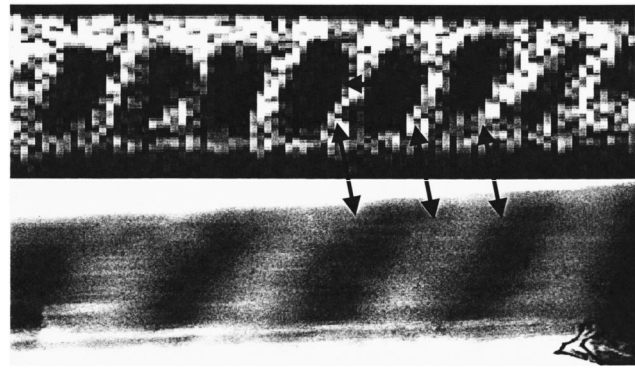


Fig. 4 OCT (top) and OM image comparison and measurement of crimp band period. The two images were obtained from the same location on a single fascicle. The top image is an OCT image and the bottom is from OM. The vertical arrows indicate that a bright band appears in the OCT image at the same location on the fascicle that a transition between light and dark bands occurs in the OM image. Measurements from OCT images were taken across each visible band pair as indicated by the horizontal arrow (width of horizontal arrow=110 microns).

were processed and analyzed with image processing software (Adobe Systems Inc., San Jose, CA). A median filter with a radius of one pixel was applied to each OCT image. A threshold value was then determined from inspection and applied consistently to all images from a single fascicle, converting the grayscale images to binary (black and white) images to clearly define the banding. For each OCT image taken in the zero-load configuration, a number of consecutive band pair widths (4–11) were identified and measured (Fig. 4) along the centerline. The measurement was repeated at each increment of strain for which any of the band pair widths were still visible. The average banding period was calculated at each strain level by summing the band pair widths and dividing by the number of visible band pairs. When a band pair disappeared between other pairs, a single measurement was taken across both previously visible pairs. A second average was calculated that excluded the “merged” measurements. A one-way repeated measures ANOVA was performed on all data for the first six strain increments (0–2.5 percent) using the maximum period measurement for bands that disappeared. Post-hoc Tukey tests were then performed to assess the individual differences between strain levels.

Results

There was a two-to-one relationship between the banding period seen in OCT images and the crimp period seen in OM images (Fig. 4). Stress-strain data from eight fascicles were successfully obtained for strain increments from 0 to 5 percent with the anticipated behavior. Crimp data were continuously tracked at strain increments from 0 percent to a minimum of 1 percent and a maximum of 2.5 percent. These data provided insight into the behavior of crimp during uniaxial extension. Average crimp period increased until crimp disappeared while individual crimp periods both increased and decreased.

Relationship Between OCT and OM Images. The appearance of OCT images was similar to OM images, in that both showed a banding with variable period. Side-by-side comparison of the OCT bands and OM bands revealed a two-to-one relationship (Fig. 4). At each transition from a light to dark or a dark to light band in an OM image, a bright band appeared in the OCT image. Average OCT band measurements from images taken with the slide parallel and perpendicular to the imaging beam axis differed from each other by less than the resolution of the OCT system.

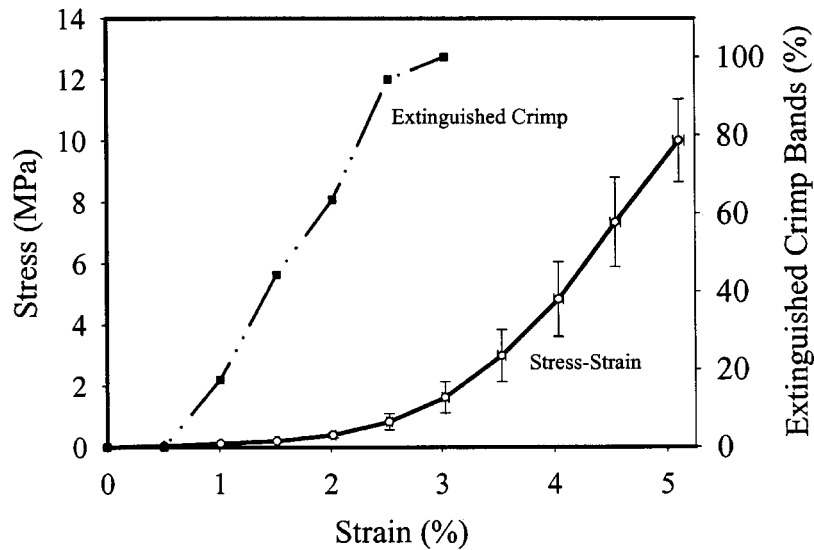


Fig. 5 Average stress-strain curve for all fascicles tested (mean \pm SEM, $N=8$ fascicles) and percent of crimp bands extinguished as a function of applied tensile strain

Stress-Strain Behavior. The stress-strain data exhibited the characteristic nonlinear behavior of collagenous soft tissues. The average cross-sectional area of the fascicles was 0.078 ± 0.023 mm². At a given strain level, stress values were lower than the expected range reported in the literature (19 to 40 MPa at 5 percent strain [20,21], Fig. 5). The toe region of the curve was longer than that documented in the study by Price et al. [21].

Individual Crimp Changes With Applied Strain. Crimp periods began to disappear individually rather than simultaneously along the length of the fascicle or successively from the ends toward the center, as might be expected if strain distribution was higher toward the clamped ends. Intermittently, single periods disappeared before the whole. Crimp periods always disappeared

completely before 3 percent axial strain was reached (Fig. 5) and a 95 percent confidence interval of 2.0 to 2.8 percent strain was calculated for complete band extinction. Banding at the surface of the fascicle was visually observed to disappear sooner than along the center axis. Nonuniform variations in single crimp periods occurred in each straining sequence, both increasing and decreasing (Figs. 6 and 7).

Average Crimp Changes With Applied Strain. Average OCT band period was plotted against applied strain to determine the correlation between strain level and crimp period. As strain increased, the average band period (and therefore crimp period) also increased (Fig. 8). The increase in average band period with applied tensile strain was nonlinear. When measurements for pe-

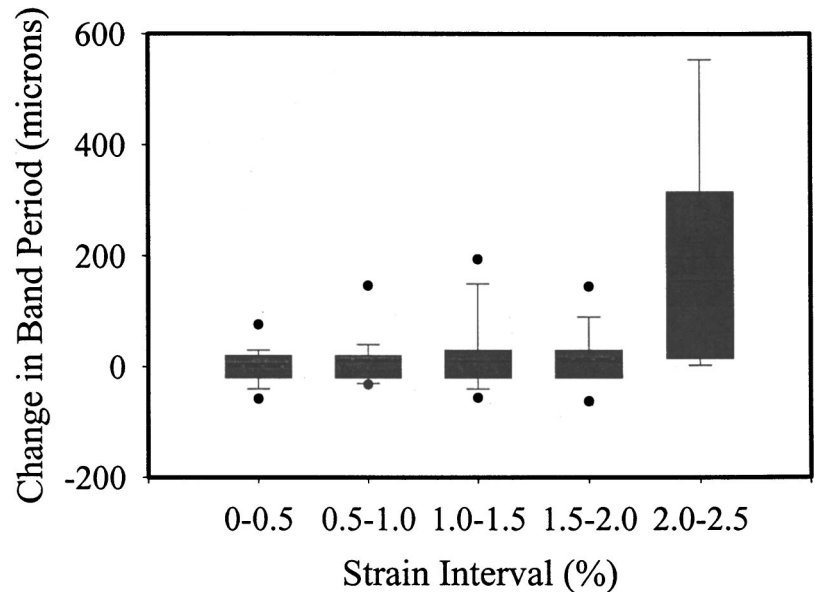


Fig. 6 Box plot of the change in crimp band widths, showing both positive and negative changes and their distribution. Boxes are 25th to 75th percentile, whiskers show the 10th and 90th percentile, dashed lines show the means, solid lines show the medians, and the circles are the 5th and 95th percentiles.

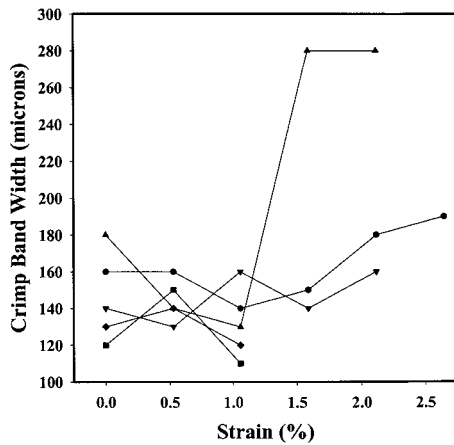


Fig. 7 Crimp lengths tracked for a single sample as a function of applied tensile strain

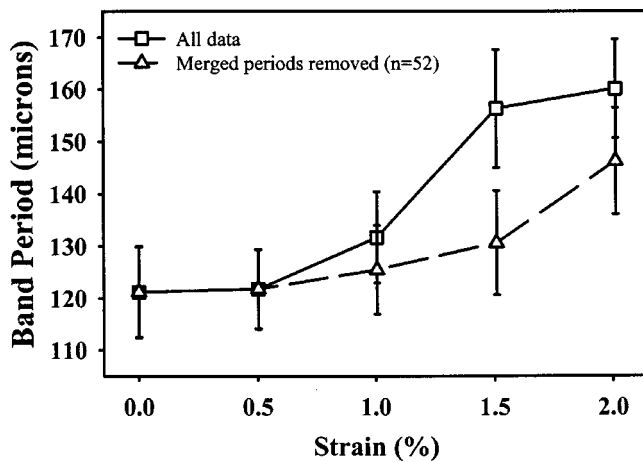


Fig. 8 Average band period as a function of applied tensile strain. Mean \pm SEM, $N=52$ band pair periods.

riods that had merged with other periods were omitted from the average, the increase in the average was still non-linear, but the curve was smoother. The data point at 2.5 percent strain is not shown since only three period measurements were available at this strain level. The one-way repeated measures ANOVA showed a significant effect of strain level on band period length ($p < 0.001$). Post-hoc Tukey tests demonstrated that the band period at 1.5 percent was greater than 0 percent, the band period at 2 percent was greater than 0.0, 0.5, and 1.0 percent, and the band period at 2.5 percent was greater than 0.0, 0.5, 1.0, 1.5, and 2.0 percent. All other comparisons showed no difference.

Discussion

This study utilized OCT imaging to measure changes in tendon crimp during uniaxial extension. The comparison of OCT and OM images facilitated the interpretation of the OCT bands in relation to crimp period. The results may also aid the mathematical modeling of ligament and tendon material behavior.

OM studies of fascicle crimp have shown that image banding occurs due to the orientation of the fibrils in relation to the incident light [8]. A similar phenomenon occurs in OCT images. The comparison between OCT and OM images clarified the manner in which the OCT imaging beam interacts with the crimped fibrils. OCT depends on reflected light rather than transmitted light. More light is reflected when the fibrils are aligned perpendicular to the

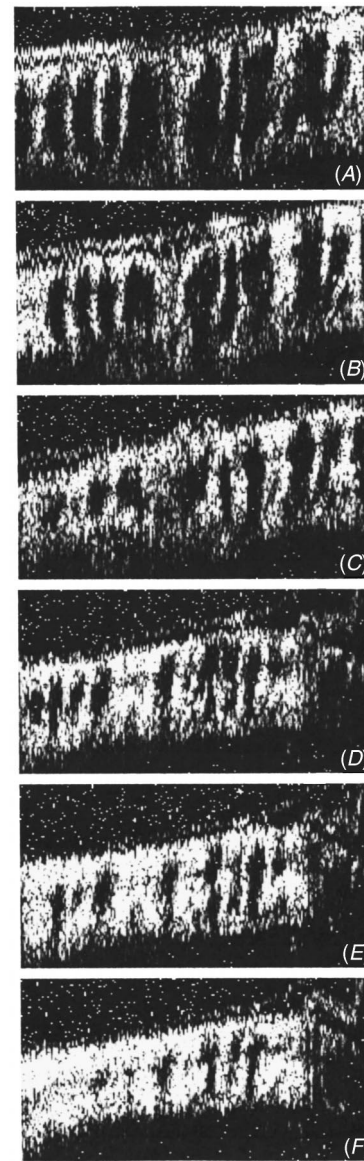


Fig. 9 OCT image sequence for rat tail fascicle under tensile strains of (A) 0 percent, (B) 0.5 percent, (C) 1.0 percent, (D) 1.5 percent, (E) 2.0 percent, and (F) 2.5 percent. Bands first began to disappear on the outer edges. Horizontal image size=2000 microns, vertical image size=350 microns.

beam. Strong reflections consequently occur at the crests and troughs of the crimp waveform. The band period measured in OCT images is therefore equivalent to half of a crimp period. Some variation between OCT and OM measurements of crimp period may occur due to the difference in the volume of tissue being imaged. An OM image is a projection of the whole tissue, while an OCT image is a cross section of the tissue with a thickness equal to the lateral resolution ($14 \mu\text{m}$ in this case). OM images produce an average of all crimp planes in the tissue. OCT images provide a local measurement of crimp. The individual disappearance of crimp periods suggests that there is nonuniform recruitment of crimp along the length of the fascicle. This important observation needs further investigation as it may have significant implications in the understanding of mechanical behavior in the toe region.

As mentioned in the introduction, Kastelic et al. [1] suggested that fibrils are arranged in planes and cylindrically packed to form a fascicle and that the crimping plane for a given fibril is approximately normal to the radius from the fascicle center and that

crimping angle decreases with decreasing radius. Kastelic et al. [22] presented a model called SSL (sequential straightening and loading) based on the foregoing morphological assumption, in which only straightened fibrils produce resistance to strain. In this model, he hypothesized that the inner fibrils straightened first, inducing the onset of the stress-strain curve, and sequential straightening occurred toward the outer edge of the fascicle. Crimped fibrils were assumed to have negligible resistance to extension. Our observations agree with a radially sequential fibril straightening theory, only the sequence of straightening appears to be from the outside toward the center (Fig. 9), leaving the center crimp visible the longest. Our observations support a structural composition theory of cylindrically packed fibril planes, based on the ability to consistently and easily obtain an image with banding that was continuous across the width of the fascicle without preferentially choosing a specific rotational orientation about the long axis of the fascicle. Our observations also indicate that fascicle cross section is elliptical in the “free” (removed from epitenon) state, as opposed to circular or triangular.

The average crimp period changes calculated for all data is higher than is physically possible. Assuming small crimp angles (on the order of 25 deg [6]), if no (or very little) elongation occurs in the fibrils before the crimp disappears, then the expected length change would be $(L_0 \cos(25) - L_0)$. However, the average measured change was greater than this amount. This may be due to the method of measuring across two periods that appear to merge into one large period while only accounting for the one period measurement in the average. When merged period measurements were removed from the average calculation, the increase in the average was much smaller and more realistic. The change in average period between 0 and 2 percent strain was about 20 percent. Most crimp had disappeared beyond 2.0 percent strain. This suggests that crimp angles were close to 33 deg.

It is difficult to accurately determine the initial onset of stress and strain when testing tissues as small as tendon fascicles (approximately 300 microns in diameter). Kastelic et al. [22] reported that stress at the beginning of the stress-strain curve is of such low magnitude that there is ambiguity, even with very sensitive load transducers. This may explain differences between the reported stress-strain values in the literature. Kastelic considered the point of the initial onset of loading to be when the specimen first appeared to be taut. Others [21] began their measurements of strain once the crimp disappeared. In the present study, small loads were distinguishable just before the fascicle appeared taut. Considering these observations, it is not surprising that the presently reported stress-strain data are lower than data in the literature. This also explains the relatively long toe region in our data in comparison with the literature. If the data reported by Price et al. is adjusted to consider for an additional 2 percent strain experienced prior to removing crimp, then the two data sets are in agreement.

Future work should include a more rigorous characterization of the interaction between a short coherence length light source and birefringent fibers of varying orientation. The ability to image from different rotations about the fiber axis is needed as well as a side-by-side comparison with OM at each strain level. Quantitative control of the polarization state of the incident light is also needed, although images taken with a polarization sensitive OCT (PS-OCT) system revealed that the appearance of banding is not altered when changing between perpendicularly oriented polarization states (unpublished data). The coherence length of the laser source currently limits resolution, but a femtosecond laser [23] can improve resolution to 1–3 microns at a substantially increased cost for system construction.

This study has demonstrated that OCT is capable of visualizing crimp changes during uniaxial extension and that crimp period

increases with applied strain in a non-linear fashion. Crimp recruitment was non-uniform along the length of the fascicle and complete straightening occurred from the outside of the fascicle toward the center.

Acknowledgments

Support by National Science Foundation grant no. 9978820 (JKB,KAH), a Whitaker Foundation Transition Grant (JAW,KAH), and NIH grant no. AR47369 (JAW) is gratefully acknowledged.

References

- [1] Kastelic, J., Galeski, A., and Baer, E., 1978, “The Multicomposite Structure of Tendon,” *Connective Tissue Research*, **6**, pp. 11–23.
- [2] Niven, H., Baer, E., and Hiltner, A., 1982, “Organization of Collagen Fibers in Rat Tail Tendon at the Optical Microscope Level,” *Collagen Related Research*, **2**, pp. 131–142.
- [3] Rowe, R. W. D., 1985, “The Structure of Rat Tail Tendon,” *Connective Tissue Research*, **14**, pp. 9–20.
- [4] Rowe, R. W. D., 1985, “The Structure of Rat Tail Tendon Fascicles,” *Connective Tissue Research*, **14**, pp. 21–30.
- [5] Rigby, B. J., Hirai, N., Spikes, J. D., and Eyring, H., 1959, “The Mechanical Properties of Rat Tail Tendon,” *J. Gen. Physiol.*, **43**, pp. 265–289.
- [6] Diamant, J., Keller, A., Baer, E., Litt, M., and Arridge, R. G. C., 1972, “Collagen; Ultrastructure and Its Relation to Mechanical Properties as a Function of Ageing,” *Proc. R. Soc. London, Ser. B*, **180**, pp. 293–315.
- [7] Viidik, A., Danielsen, C. C., and Oxlund, H., 1982, “On Fundamental and Phenomenological Models, Structure and Mechanical Properties of Collagen, Elastin and Glycosaminoglycan Complexes,” *Biorheology*, **19**, pp. 437–451.
- [8] Gathercole, L. J., and Keller, A., 1991, “Crimp Morphology in the Fibre-Forming Collagens,” *Matrix*, **11**, pp. 214–234.
- [9] Sacks, M. S., Smith, D. B., and Hiester, E. E., 1997, “A Small Angle Light Scattering Device for Planar Connective Tissue Microstructural Analysis,” *Ann. Biomed. Eng.*, **25**, pp. 678–689.
- [10] Hsu, E. W., Muzikant, A. L., Matulevicius, S. A., Penland, R. C., and Henriquez, C. S., 1998, “Magnetic Resonance Myocardial Fiber-Orientation Mapping With Direct Histological Correlation,” *Am. J. Physiol.*, **274(5 Pt 2)**, pp. H1627–1634.
- [11] Hsu, E. W., and Setton, L. A., 1999, “Diffusion Tensor Microscopy of the Intervertebral Disc Annulus Fibrosus,” *Magn. Reson. Med.*, **41**, pp. 992–999.
- [12] Caspers, P. J., Lucassen, G. W., Wolthuis, R., Bruining, H. A., and Puppels, G. J., 1998, “In Vitro and In Vivo Raman Spectroscopy of Human Skin,” *Biospectroscopy*, **4(5 Suppl)**, pp. S31–39.
- [13] Huang, D., Swanson, E. A., Lin, C. P., Schuman, J. S., Stinson, W. G., Chang, W., Hee, M. R., Flotte, T., Gregory, K., Puliafito, C. A. et al., 1991, “Optical Coherence Tomography,” *Science*, **254(5035)**, pp. 1178–1181.
- [14] Schmitt, J. M., Yablowsky, M., and Bonner, R. F., 1995, “Subsurface Imaging of Living Skin With Optical Coherence Microscopy,” *Dermatology*, **191**, pp. 93–98.
- [15] Barton, J. K., Milner, T. E., Pfefer, T. J., Nelson, J. S., and Welch, A. J., 1997, “Optical Low-Coherence Reflectometry to Enhance Monte Carlo Modeling of Skin,” *J. Biomed. Opt.*, **2(2)**, pp. 226–234.
- [16] Brezinski, M. E., Tearney, G. J., Brett, B. E., Boppart, S. A., Hee, M. R., Swanson, E. A., Southern, J. F., and Fujimoto, J. G., 1996, “Imaging of Coronary Artery Microstructure With Optical Coherence Tomography,” *Am. J. Cardiol.*, **77**, pp. 92–93.
- [17] de Boer, J. F., Milner, T. E., van Gemert, M. J. C., and Nelson, J. S., 1997, “Two-Dimensional Birefringence Imaging in Biological Tissue by Polarization-Sensitive Optical Coherence Tomography,” *Opt. Lett.*, **22**, pp. 934–936.
- [18] Kwan, M. K., and Woo, S. L-Y., 1989, “A Structural Model to Describe the Nonlinear Stress-Strain Behavior for Parallel-Fibered Collagenous Tissues,” *ASME J. Biomech. Eng.*, **111**, pp. 361–363.
- [19] Hurschler, C., Loitz-Ramage, B., and Vanderby, Jr., R., 1997, “A Structurally Based Stress-Stretch Relationship for Tendon and Ligament,” *ASME J. Biomech. Eng.*, **119**, pp. 392–399.
- [20] Betsch, D. F., and Baer, E., 1980, “Structure and Mechanical Properties of Rat Tail Tendon,” *Biorheology*, **17**, pp. 83–94.
- [21] Price, J. P., Njus, G. O., and Conway, T. A., 1996, “Ultrastructural Properties of Rat Tail Tendon,” *Proc., Fifteenth Southern Biomedical Engineering Conference*, 456–459.
- [22] Kastelic, J., Palley, I., and Baer, E., 1980, “A Structural Mechanical Model for Tendon Crimping” *J. Biomech.*, **13**, pp. 887–893.
- [23] Drexler, W., Morgner, U., Kartner, F. X., Pitris, C., Boppart, S. A., Li, X. D., Ippen, E. P., and Fujimoto, J. G., 1999, “In Vivo Ultrahigh-Resolution Optical Coherence Tomography,” *Opt. Lett.*, **24(17)**, pp. 1221–1223.